Resolved-sideband cooling of a single ^{9}Be$^+$ ion in a cryogenic multi-Penning-trap for discrete symmetry tests with (anti-)protons

Juan M. Cornejo [1,*] Johannes Brombacher [1] Julia A. Coenders,[1] Moritz von Boehn [1] Teresa Meiners [1]
Malte Niemann,[1] Stefan Ulmer [2,3] and Christian Ospelkaus [1,4]

[1]*Institut für Quantenoptik, Leibniz Universität Hannover, Welfengarten 1, 30167 Hannover, Germany*
[2]*RIKEN, Ulmer Fundamental Symmetries Laboratory, 2-1 Hirosawa, Wako, Saitama 351-0198, Japan*
[3]*Institut für Experimentalphysik, Heinrich Heine Universität Düsseldorf, Universitätsstr. 1, 40225 Düsseldorf, Germany*
[4]*Physikalisch-Technische Bundesanstalt, Bundesallee 100, 38116 Braunschweig, Germany*

Manipulating the motion of individual trapped ions at the single quantum level has become standard practice in radio-frequency ion traps, enabling sweeping advances in quantum information processing and precision metrology. The key step for motional-state engineering is ground-state cooling. Full motional control also bears great potential to explore another regime of sensitivities for fundamental physics tests in Penning traps. Here we demonstrate the key enabling step by implementing resolved-sideband cooling on the axial mode of a single ^{9}Be$^+$ ion in a 5 Tesla cryogenic Penning trap. The system has been developed for the implementation of high-precision antimatter experiments to test the fundamental symmetries of the standard model with the highest accuracy in the baryonic sector. We measure an axial phonon number of $\bar{n}_z = 0.10(4)$ after cooling and demonstrate that the axial heating rate in our system is compatible with the implementation of quantum logic spectroscopy of (anti-)protons.

Penning-trap-based tests of fundamental physics rely on the measurement of motional and internal frequencies of the trapped particle [1–3]. A strong magnetic field B and a weak electrostatic potential ϕ define the motional and internal frequencies [4], and fundamental properties of the trapped particles can be studied by measuring frequency ratios, such that the magnetic field cancels out to lowest order [5]. In the pursuit of today's most precise measurements, the majority of significant systematic frequency shifts and their related uncertainties can be attributed to the finite energy of the confined particle. Along its trajectory, the particle interacts with imperfections in the trapping fields [6], all the while adhering to the principles of special relativity [7]. This results in energy-dependent frequency shifts and introduces uncertainties in the measured frequency ratios [8]. While notable progress has been made in enhancing the attainable uniformity of the technical trapping fields [5,9], the particle's localization remains an area with considerable potential for further improvement. Present precision experiments exclusively rely on the coupling of the particle's motion to a sensitive cryogenic superconducting detection circuit [10] that defines the detection interface to investigate the fundamental particle properties. In addition, the circuit cools and localizes the particle, implying in most

cases a thermal state of motion, with an effective mean energy that is close to the physical circuit temperature of a few Kelvin.

Ultrahigh-precision experiments using Penning traps will greatly benefit from the reduction of systematic errors offered by full motional control over atomic ions, with applications to atomic masses [11,12] and *g*-factor measurements [13,14] or related tests of fundamental physics [15,16]. Motional control at the single-quantum level is the instrumental step for establishing quantum logic spectroscopy [17] in Penning traps, a technique that has enabled a class of precision measurements in radio-frequency ion traps, where manipulating individual trapped ions at the single quantum level has become standard practice [18], enabling applications ranging from quantum information processing [19–21] to precision metrology [22].

The key ingredient for full control is the ability to ground-state cool the motion of the particle in the trap through resolved-sideband laser cooling. Laser cooling not only provides localization of the particle at the quantum limit, it also does so on much shorter timescales of milliseconds compared to minutes up to hours for resonator-based resistive cooling, as used in current state-of-the-art Penning trap experiments [13]. The challenge is that most species of interest in Penning-trap precision measurements—such as antiprotons, protons, light nuclei, and highly charged ions—cannot be readily laser-cooled directly, and that the large magnetic field of the Penning trap complicates cooling significantly for those that can be laser cooled [23–25]. The former can be addressed by implementing sympathetic cooling schemes [20,26–31].

Regarding laser cooling, pioneering experiments on Doppler cooling were carried out in a Penning trap [32];
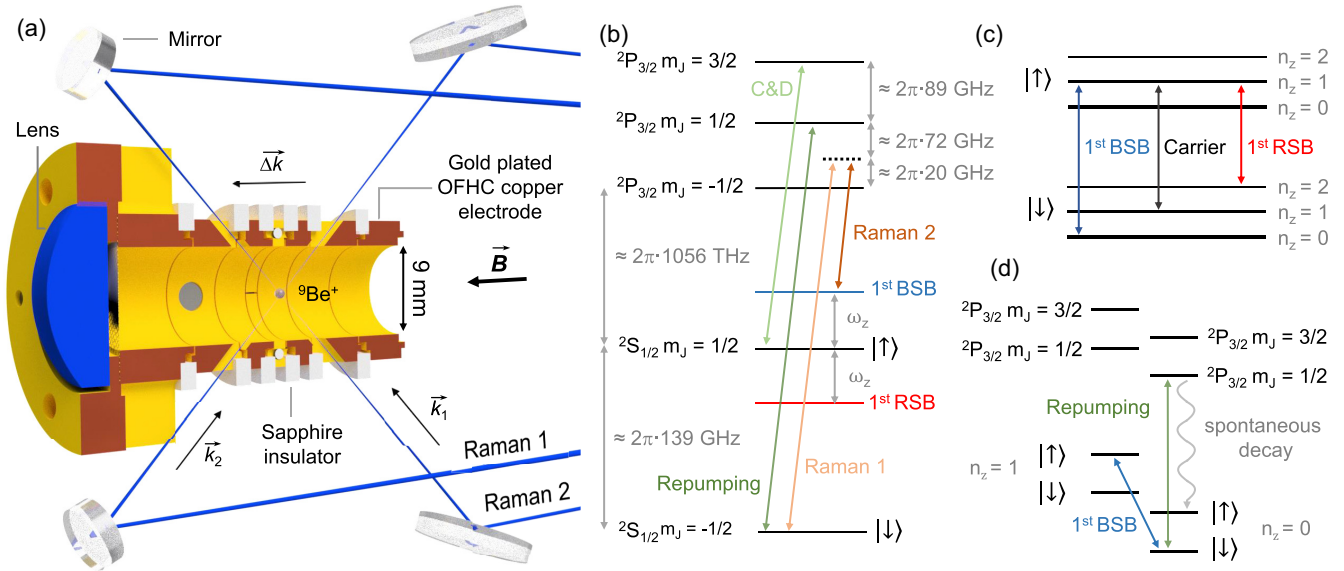
FIG. 1. (a) Cross-section view of the cryogenic trap. Electrodes are cylinder-shaped and made of gold-plated oxygen-free high thermal conductivity (OFHC) copper of 9 mm inner diameter, electrically insulated by sapphire rings. A lens is used to collect the fluorescence photons emitted by a single laser-cooled ^{9}Be$^+$ ion. Four mirrors are used to guide the laser beams into the trap. The Raman laser beams are guided in a 90°crossed-beam configuration resulting in an effective wave-vector difference along the axial direction. The cooling and repumper laser beams (not shown) use the same path as the Raman 2 laser beam. (b) Relevant internal energy levels scheme of ^{9}Be$^+$ in a 5 Tesla magnetic field. The cooling and detection (C&D) as well as the repumper transition are represented by light and dark green arrows, respectively. The Raman transitions are depicted by dark and light orange for Raman lasers 1 and 2, respectively. The presence of sidebands is indicated by the red and blue levels below and above of the spin $|\uparrow\rangle$ state, respectively. (c) The quantized motional energy levels of the axial mode $n_z = 0$, $n_z = 1$, and $n_z = 2$ are represented for both spin states $|\uparrow\rangle$ and $|\downarrow\rangle$. The carrier and the first blue and red sidebands are depicted by black, blue, and red arrows, respectively. (d) Simplified internal energy level scheme represented for motional energies of $n_z = 1$ and $n_z = 0$. The repumper and the first blue sideband transitions are depicted by dark green and blue arrows, respectively. During the repumper pulse, the ion is reset to the $|\uparrow\rangle$ state after spontaneous decay, which is represented by the curved gray arrow. Energy levels are not drawn to scale.

however, later developments on ground-state cooling, motional-state synthesis, and quantum logic heavily focused on radio-frequency Paul traps. Recent years have seen growing interest in motional-state engineering in Penning traps because of challenging applications in metrology and fundamental tests (see discussion above), but also because of interesting ideas in quantum logic and quantum control [17,20,33]. However, the large magnetic field of the Penning trap complicates cooling significantly [23–25]. A key experimental step was the realization of ground-state cooling of a single ^{40}Ca$^+$ ion in a Penning trap at Imperial College [23]. NIST subsequently demonstrated cooling of the collective motion of many ions to the motional ground state [24]. At ETH, a Penning-trap architecture for quantum logic was recently demonstrated, including ground-state cooling of single ^{9}Be$^+$ ions in a surface-electrode Penning trap [34]. For sympathetic cooling in Penning-trap precision measurements on (anti-)protons, light nuclei, and highly charged ions, it is desirable to use a species with a charge-to-mass ratio as high as possible, highly favoring ^{9}Be$^+$. However, present results on ^{9}Be$^+$ are not directly applicable here. The surface-electrode Penning trap lacks the high degree of symmetry that is typically required in Penning-trap precision measurements and cannot be easily interfaced with beam-line sources of rare species. Compared to cooling the collective motion of a crystal, single-ion cooling for precision experiments is significantly complicated because of the constraints from cryogenic operation and laser beam delivery,

combined with the much more stringent requirements on Doppler cooling.

In this paper, we report on a cryogenic Penning trap setup that has been designed to probe the fundamental *CPT* symmetry with (anti-)protons and explore a regime of accuracies that will become possible through full motional control enabled through sympathetic ground-state cooling with a ^{9}Be$^+$ ion. We have previously presented the experimental setup [35], discussed protocols for implementing sympathetic cooling and quantum logic spectroscopy based on the proposal by Heinzen and Wineland [26], demonstrated a method to implement spin-motional control for sideband transitions [36,37] and resolved-sideband spectroscopy [38] as well as fast adiabatic transport [39]. Here we demonstrate motional-ground state cooling in this setup as the key step that will enable full motional control and quantum logic spectroscopy of single (anti-)protons.

Our cryogenic Penning trap system is located at the center of a superconducting magnet with a magnetic field strength $B = 5$ T to store a single ^{9}Be$^+$ ion [35,38]. Among the different traps in our experiment stack, only the so-called beryllium trap is used for laser manipulation of ions. It is depicted in Fig. 1(a). The electric field produced by the trap electrodes in conjunction with the axial magnetic field $\vec{B}$ are used to confine the charged particle in the trap. From a classical point of view, the motion of the trapped ion is described by an axial mode with a frequency ν_z and two radial modes, the so-called magnetron and reduced cyclotron modes, with frequencies

ν_- and ν_+, respectively. These frequencies are related to the free cyclotron frequency $\nu_c = qB/(2\pi m)$ by the invariance theorem $\nu_c^2 = \nu_+^2 + \nu_z^2 + \nu_-^2$ [40], where q/m is the charge-to-mass ratio of the trapped particle.

Once a single $^9\mathrm{Be}^+$ ion is stored in the trap [35,41], Doppler cooling is performed on the ion [38]. Figure 1(b) shows the relevant energy levels for a $^9\mathrm{Be}^+$ ion in a 5 Tesla magnetic field as well as the laser-induced transitions. A Doppler cooling and detection laser resonant with the $|^2S_{1/2}, m_j = +1/2\rangle \rightarrow |^2P_{3/2}, m_j = +3/2\rangle$ transition is used to cool the ion. A repumper laser resonant with the $|^2S_{1/2}, m_j = -1/2\rangle \rightarrow |^2P_{3/2}, m_j = +1/2\rangle$ transition prevents the accumulation of population in $|^2S_{1/2}, m_j = -1/2\rangle$.

Two Raman laser beams with a detuning of $\approx 20\,\mathrm{GHz}$ from the $|\!\downarrow\rangle \equiv |^2S_{1/2}, m_j = -1/2\rangle \rightarrow |^2P_{3/2}, m_j = -1/2\rangle$ and $|\!\uparrow\rangle \equiv |^2S_{1/2}, m_j = +1/2\rangle \rightarrow |^2P_{3/2}, m_j = -1/2\rangle$ transitions, called Raman 1 and 2, respectively, are used to drive a two-photon stimulated Raman spin-flip transition between the two "qubit" states [20] $|\!\downarrow\rangle$ and $|\!\uparrow\rangle$ with an energy difference $h\nu_0 \approx h \times 139\,\mathrm{GHz}$. To simultaneously address a motional mode of the trapped ion, the Raman laser beams must fulfill the resonance condition given by the effective Hamiltonian of the transition [20,36,38]. For this, the Raman laser beams also need to exhibit a wave-vector difference $\vec{\Delta k} = \vec{k}_1 - \vec{k}_2$ with a finite projection on the axial direction to be able to address the axial motion as shown in Fig. 1(a). In addition, the Raman laser beams' frequency difference $\nu_R = \nu_1 - \nu_2$ must satisfy the specific resonance condition $\nu_R = \nu_0 + m \cdot \nu_z$, where m is an integer. For $m = 0$, the Raman lasers address the carrier transition at ν_0. For $m \neq 0$, a motional sideband spectrum around the carrier transition is expected. Transitions with $m > 0$ $(m < 0)$ are known as blue (red) sideband transitions. After Doppler cooling, the ion is expected to be in a thermal state of motion. If a mean phonon number much larger than one is obtained, the motional sideband spectrum will follow a Doppler broadened envelope determined by the ion temperature [36,42].

Before implementing sideband cooling, we identify the proper sideband transitions and frequencies as described in Ref. [38]. Compared to Ref. [38], where an axial frequency of 435 kHz and a Doppler detuning of 20 MHz below resonance had been chosen, here an axial frequency of 693 kHz and a Doppler detuning of 15 MHz below resonance is used. This facilitates ground-state cooling for two reasons: the number of potentially involved sideband transitions is reduced, as well as the number of required pulses. Working with this parameter set only became possible after improvements related to laser beam position stability and ion loading protocols. Using these parameters, we estimate a mean phonon number of around $\bar{n}_z \approx 60$, which corresponds to an estimated temperature of around 2.0 mK in the axial mode after Doppler cooling, similar to the 1.77(10) mK measured in Ref. [36]. This is about 3.5 times the theoretically achievable Doppler limit of $\approx 0.5\,\mathrm{mK}$. Possible reasons for not reaching the Doppler limit are related to the complicated cooling dynamics of a single $^9\mathrm{Be}^+$ in Penning traps and have already been discussed in Refs. [36,38].

Sideband cooling proceeds as follows: Each motion-reducing blue sideband pulse is followed by a repumper pulse of duration 20 µs to reset the spin to $|\!\uparrow\rangle$. The sideband interaction strength depends on the phonon number n of the axial motion [20]; in particular, the sideband interaction strength of all sideband transitions vanishes close to certain phonon numbers [20] across the range of relevant phonon numbers for our value of $\bar{n}_z$. It is therefore not sufficient to apply only first-order sideband transitions for cooling because motional state population would get stuck around phonon numbers where the first-order sideband interaction strength vanishes.

We therefore start by applying alternating sixth- and fifth-order blue sideband pulses. The application of the sideband pulses in alternating order is favorable because the odd order sideband interaction strength tends to vanish for phonon numbers where the even order sideband interaction strength is significant and vice versa [43]. After 20 alternating sideband pulse pairs on the sixth- and fifth-order blue sidebands, we apply two more sequences of 20 alternating sideband pulse pairs on the fourth-/third- and second-/first-order blue sidebands each. It is found experimentally that the most robust results were obtained by applying all sideband pulses for the same interaction time.

After the sideband cooling sequence, we apply a sideband analysis pulse (frequency difference ν_R between the two Raman beams) for a given interaction time to determine the strengths of the motional sidebands and obtain information about the motional-state occupation. Afterward, we turn on the cooling laser; if the ion is bright (scatters photons from the laser beam), it is determined to be in the $|\!\uparrow\rangle$ state, and in $|\!\downarrow\rangle$ otherwise. Following the detection, the repumper laser beam is applied to reset the spin state to $|\!\uparrow\rangle$. By stepping ν_R of the analysis pulse around the motional sideband frequencies and repeating the experiment, we obtain a sideband spectrum.

The pulse sequence described above is able to cool a single $^9\mathrm{Be}^+$ ion close to the motional ground state of the axial mode of motion. Figure 2 shows the excitation probability of the first red and blue sideband analysis pulse after the cooling sequence. For the presented measurements, both beams are focused to a beam waist of around 150 µm at the ion position and the laser power stabilized to 5 mW and 1.7 mW for Raman lasers 1 and 2, respectively. The difference in power is due to the required polarization of each Raman transition [36]. The sideband interaction time for each sideband cooling pulse was 10 µs. The total of 120 sideband cooling pulses of 10 µs each and of 120 repump pulses of 20 µs each therefore took 3.6 ms. The sideband interaction time for the red and blue sideband analysis pulse was 10 µs. From the ratio of the maximum excitation probability of both first-order sidebands (see Fig. 2), an average phonon number in the axial mode of $\bar{n}_z = 0.10(4)$ is obtained. To demonstrate that there is no significant occupation of higher phonon states, we also measured the second-order blue and red sidebands, showing negligible excitation probability for the motion-removing second order sideband (see Appendix).

To test our ability to perform coherent state manipulation, Rabi oscillations on the first red sideband after Doppler and sideband cooling were analyzed. Figure 3 shows the excitation probability for different interaction times of the red sideband analysis pulse on resonance with the first red sideband. A sinusoidal exponential decay is fitted to the data, yielding a frequency of 61(2) kHz and a decay time of 10(2) µs.
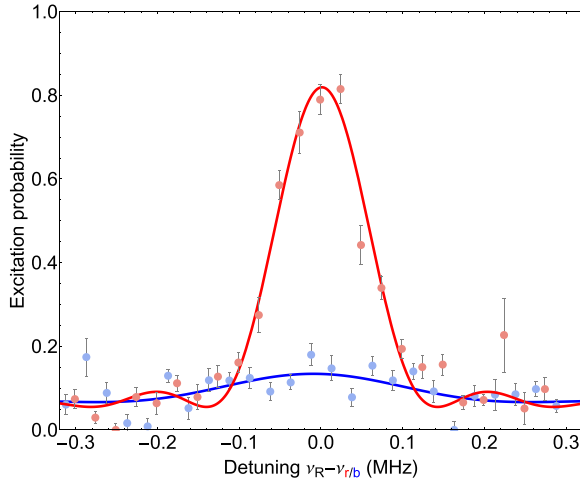
FIG. 2. The excitation probability is shown as a function of the Raman laser beams' detuning. Data is depicted by blue and red dots for the first blue and red sidebands, respectively. Each data point and error bars are obtained from 100 measurements per data point. The blue and red lines are sinc-squared function fits to the data for the first blue and red sidebands. The center frequency of each transition is represented at zero detuning for clarity, where $\nu_{r/b}$ represents 138.911076 GHz and 138.912490 GHz for the first blue sideband and the first red sideband, respectively.

We assume that small variations in position of the Raman laser beams are the main causes of decoherence. While small changes in cooling pulse time were experimentally observed to not affect the cooling performance as judged by the resulting sideband spectrum, we expect fluctuations on that order to significantly decohere the sideband flopping data. Similar behavior was observed in our setup before in a copropagating Raman configuration [38]. This issue will be addressed by an active position stabilization system for both Raman laser beams.

One important aspect for the implementation of quantum logic spectroscopy in this system is to examine the
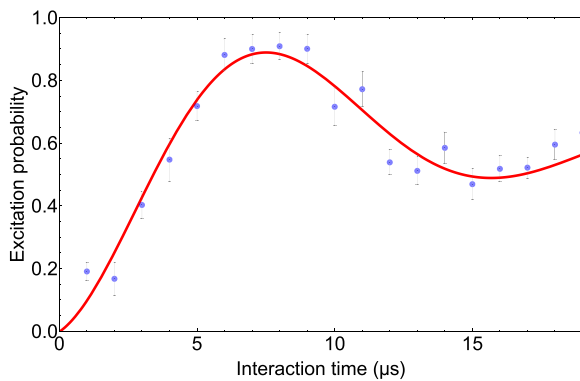

FIG. 3. The excitation probability is shown as a function of the interaction time. Data are depicted by blue dots. Data and error bars are obtained from 100 measurements. The red line is a fit to the data using a sinusoidal exponential decay.
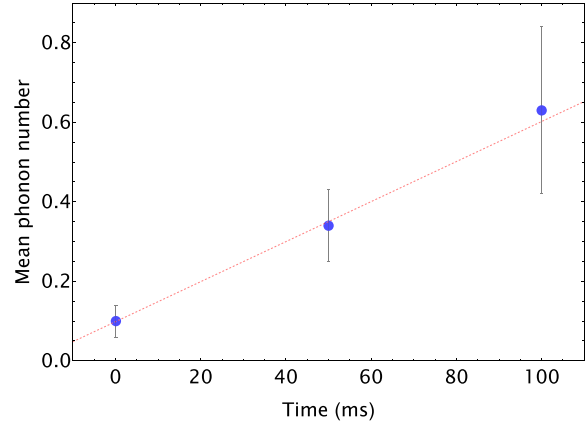

FIG. 4. Heating rate measurement of the axial mode of a single laser-cooled ^{9}Be$^+$ ion in our Penning trap system at an axial frequency of 693 kHz. The mean phonon number is measured after sideband cooling for a delay time of 10 μs, 50 ms, and 100 ms. Data are depicted by blue dots. The dashed red line is a linear fit to the data. The observed heating rate is compatible with the implementation of quantum logic spectroscopy in this setup as a logical next step.

rate at which the axial motion gains energy when otherwise left alone. We measure this key quantity by recording first blue and red sideband spectra following a variable delay time introduced after sideband cooling. Figure 4 shows the mean phonon number as a function of this delay time. From the linear fit to the data in Fig. 4, a heating rate of $\dot{n}_z = (5.0 \pm 0.3)$ quanta/s is obtained. This corresponds to a noise spectral density scaled by the trap frequency of $\omega_z S_E(\omega_z) = 4m\hbar\omega_z^2 \dot{n}_z/q^2 = (2.3 \pm 0.1) \times 10^{-8}$ V/m^2, where $\omega_z = 2\pi\nu_z$ and $\hbar$ is the reduced Planck's constant. While still limited by technical noise, e.g., on the voltage sources for the electrodes, this measurement shows that the heating rate is low enough to implement quantum logic spectroscopy in future experiments, as all required steps for this are expected to happen on much shorter timescales.

The results shown in this paper are an instrumental step towards the implementation of quantum logic spectroscopy [17] in high-precision Penning trap experiments [33,37] with the potential to establish quantum limited measurement technology in some of the most sensitive tests of the standard model. Because *CPT* and Lorentz symmetry are closely related, an earth-based experiment would be expected to measure sidereal variations of the observables [44–46]. Such measurements would require sampling rates and accuracies that are difficult to imagine based on state-of-the-art resonator-based cooling techniques. The increased sampling rate and accuracy projected as a result of ground-state cooling and quantum logic spectroscopy would enable such effects to be probed [33]. More generally, the introduction of ground-state cooling for precision measurements in Penning traps will enable such measurements to ultimately operate at the quantum limit.

ACKNOWLEDGMENTS

APPENDIX: EXCITATION PROBABILITY OF THE SECOND RED AND BLUE SIDEBANDS

Figure 5 shows the excitation probability of the second red and blue sideband analysis pulse after the cooling sequence described in the main text. The sideband interaction time for the red and blue sideband analysis pulse was $10\,\mu s$. As shown in Fig. 2, both sidebands exhibit a high degree of asymmetry, with negligible excitation probability for the second blue sideband. This, together with the first-order sideband data, demonstrates that there is no significant population trapped in higher phonon states.
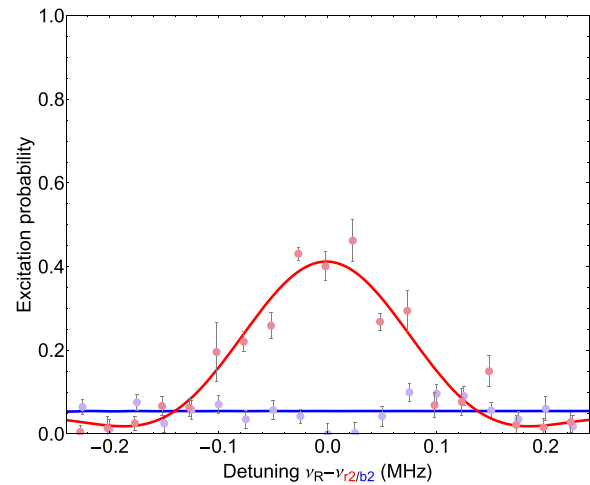

FIG. 5. The excitation probability is shown as a function of the Raman laser beams' detuning. Data is depicted by blue and red dots for the second blue and red sidebands, respectively. Data points and error bars are obtained from 100 measurements per data point. The blue and red lines are sinc-squared function fits to the data for the second blue and red sidebands. The center frequency of each transition is represented at zero detuning for clarity, where $\nu_{r2/b2}$ represents 138.910350 GHz and 138.913202 GHz for the second blue sideband and the second red sideband, respectively.

[1] K. Blaum, S. Eliseev, and S. Sturm, Perspectives on testing fundamental physics with highly charged ions in Penning traps, Quantum Sci. Technol. **6**, 014002 (2021).

[2] K. Blaum, Y. N. Novikov, and G. Werth, Penning traps as a versatile tool for precise experiments in fundamental physics, Contemp. Phys. **51**, 149 (2010).

[3] K. Blaum, High-accuracy mass spectrometry with stored ions, Phys. Rep. **425**, 1 (2006).

[4] L. S. Brown and G. Gabrielse, Geonium theory: Physics of a single electron or ion in a Penning trap, Rev. Mod. Phys. **58**, 233 (1986).

[5] C. Smorra, K. Blaum, L. Bojtar, M. Borchert, K. A. Franke, T. Higuchi, N. Leefer, H. Nagahama, Y. Matsuda, A. Mooser, M. Niemann, C. Ospelkaus, W. Quint, G. Schneider, S. Sellner, T. Tanaka, S. Van Gorp, J. Walz, Y. Yamazaki, and S. Ulmer, BASE—The baryon antibaryon symmetry experiment, Eur. Phys. J.: Spec. Top. **224**, 3055 (2015).

[6] J. Ketter, T. Eronen, M. Höcker, S. Streubel, and K. Blaum, First-order perturbative calculation of the frequency-shifts caused by static cylindrically-symmetric electric and magnetic imperfections of a Penning trap, Int. J. Mass Spectrom. **358**, 1 (2014).

[7] M. Vogel, W. Quint, and W. Nörtershäuser, Trapped ion oscillation frequencies as sensors for spectroscopy, Sensors **10**, 2169 (2010).

[8] M. J. Borchert, J. A. Devlin, S. R. Erlewein, M. Fleck, J. A. Harrington, T. Higuchi, B. M. Latacz, F. Voelksen, E. J. Wursten, F. Abbass, M. A. Bohman, A. H. Mooser, D. Popper, M. Wiesinger, C. Will, K. Blaum, Y. Matsuda, C. Ospelkaus, W. Quint, J. Walz, Y. Yamazaki, C. Smorra, and S. Ulmer, A 16-parts-per-trillion measurement of the antiproton-to-proton charge–mass ratio, Nature (London) **601**, 53 (2022).

[9] F. Heiße, S. Rau, F. Köhler-Langes, W. Quint, G. Werth, S. Sturm, and K. Blaum, High-precision mass spectrometer for light ions, Phys. Rev. A **100**, 022518 (2019).

[10] H. Nagahama, G. Schneider, A. Mooser, C. Smorra, S. Sellner, J. Harrington, T. Higuchi, M. Borchert, T. Tanaka, M. Besirli, K. Blaum, Y. Matsuda, C. Ospelkaus, W. Quint, J. Walz, Y. Yamazaki, and S. Ulmer, Highly sensitive superconducting circuits at ~700 kHz with tunable quality factors for image-current detection of single trapped antiprotons, Rev. Sci. Instrum. **87**, 113305 (2016).

[11] F. Heiße, F. Köhler-Langes, S. Rau, J. Hou, S. Junck, A. Kracke, A. Mooser, W. Quint, S. Ulmer, G. Werth, K. Blaum, and S. Sturm, High-precision measurement of the proton's atomic mass, Phys. Rev. Lett. **119**, 033001 (2017).

[12] S. Sturm, F. Köhler, J. Zatorski, A. Wagner, Z. Harman, G. Werth, W. Quint, C. H. Keitel, and K. Blaum, High-precision measurement of the atomic mass of the electron, Nature (London) **506**, 467 (2014).

[13] G. Schneider, A. Mooser, M. Bohman, N. Schön, J. Harrington, T. Higuchi, H. Nagahama, S. Sellner, C. Smorra, K. Blaum, Y. Matsuda, W. Quint, J. Walz, and S. Ulmer, Double-trap measurement of the proton magnetic moment at 0.3 parts per billion precision, Science **358**, 1081 (2017).

[14] C. Smorra, P. E. Blessing, M. J. Borchert, J. A. Devlin, J. A. Harrington, T. Higuchi, J. Morgner, H. Nagahama, S. Sellner, M. A. Bohman, A. H. Mooser, G. L. Schneider, N.

Schön, M. Wiesinger, K. Blaum, Y. Matsuda, C. Ospelkaus, W. Quint, J. Walz, Y. Yamazaki, and S. Ulmer, 350-fold improved measurement of the antiproton magnetic moment using a multi-trap method, Hyperfine Interact. **239**, 47 (2018).

[15] J. Morgner, B. Tu, C. M. König, T. Sailer, F. Heiße, H. Bekker, B. Sikora, C. Lyu, V. A. Yerokhin, Z. Harman, J. R. Crespo López-Urrutia, C. H. Keitel, S. Sturm, and K. Blaum, Stringent test of QED with hydrogen-like tin, Nature (London) **622**, 53 (2023).

[16] A. Schneider, B. Sikora, S. Dickopf, M. Müller, N. S. Oreshkina, A. Rischka, I. A. Valuev, S. Ulmer, J. Walz, Z. Harman, C. H. Keitel, A. Mooser, and K. Blaum, Direct measurement of the ^{3}He$^+$ magnetic moments, Nature (London) **606**, 878 (2022).

[17] P. O. Schmidt, T. Rosenband, C. Langer, W. M. Itano, J. C. Bergquist, and D. J. Wineland, Spectroscopy using quantum logic, Science **309**, 749 (2005).

[18] D. Leibfried, R. Blatt, C. Monroe, and D. Wineland, Quantum dynamics of single trapped ions, Rev. Mod. Phys. **75**, 281 (2003).

[19] J. I. Cirac and P. Zoller, Quantum computations with cold trapped ions, Phys. Rev. Lett. **74**, 4091 (1995).

[20] D. J. Wineland, C. Monroe, W. M. Itano, D. Leibfried, B. E. King, and D. M. Meekhof, Experimental issues in coherent quantum-state manipulation of trapped atomic ions, J. Res. Natl. Inst. Stand. Technol. **103**, 259 (1998).

[21] D. Kielpinski, C. Monroe, and D. J. Wineland, Architecture for a large-scale ion-trap quantum computer, Nature (London) **417**, 709 (2002).

[22] A. D. Ludlow, M. M. Boyd, J. Ye, E. Peik, and P. O. Schmidt, Optical atomic clocks, Rev. Mod. Phys. **87**, 637 (2015).

[23] J. F. Goodwin, G. Stutter, R. C. Thompson, and D. M. Segal, Resolved-sideband laser cooling in a Penning trap, Phys. Rev. Lett. **116**, 143002 (2016).

[24] E. Jordan, K. A. Gilmore, A. Shankar, A. Safavi-Naini, J. G. Bohnet, M. J. Holland, and J. J. Bollinger, Near ground-state cooling of two-dimensional trapped-ion crystals with more than 100 ions, Phys. Rev. Lett. **122**, 053603 (2019).

[25] M. J. Gutiérrez, J. Berrocal, J. M. Cornejo, F. Domínguez, J. J. D. Pozo, I. Arrazola, J. Bañuelos, P. Escobedo, O. Kaleja, L. Lamata, R. A. Rica, S. Schmidt, M. Block, E. Solano, and D. Rodríguez, The TRAPSENSOR facility: An open-ring 7 tesla Penning trap for laser-based precision experiments, New J. Phys. **21**, 023023 (2019).

[26] D. J. Heinzen and D. J. Wineland, Quantum-limited cooling and detection of radio-frequency oscillations by laser-cooled ions, Phys. Rev. A **42**, 2977 (1990).

[27] K. R. Brown, C. Ospelkaus, Y. Colombe, A. C. Wilson, D. Leibfried, and D. J. Wineland, Coupled quantized mechanical oscillators, Nature (London) **471**, 196 (2011).

[28] M. Bohman, V. Grunhofer, C. Smorra, M. Wiesinger, C. Will, M. J. Borchert, J. A. Devlin, S. Erlewein, M. Fleck, S. Gavranovic, J. Harrington, B. Latacz, A. Mooser, D. Popper, E. Wursten, K. Blaum, Y. Matsuda, C. Ospelkaus, W. Quint, J. Walz, and S. Ulmer, Sympathetic cooling of a trapped proton mediated by an LC circuit, Nature (London) **596**, 514 (2021).

[29] C. Will, M. Bohman, T. Driscoll, M. Wiesinger, F. Abbass, M. J. Borchert, J. A. Devlin, S. Erlewein, M. Fleck, B. Latacz, R. Moller, A. Mooser, D. Popper, E. Wursten, K. Blaum, Y. Matsuda, C. Ospelkaus, W. Quint, J. Walz, C. Smorra, and S. Ulmer, Sympathetic cooling schemes for separately trapped ions coupled via image currents, New J. Phys. **24**, 033021 (2022).

[30] T. Meiners, M. Niemann, J. Mielke, M. Borchert, N. Pulido, J. M. Cornejo, S. Ulmer, and C. Ospelkaus, Towards sympathetic cooling of single (anti-)protons, Hyperfine Interact. **239**, 26 (2018).

[31] J. M. Cornejo, M. J. Gutiérrez, E. Ruiz, A. Bautista-Salvador, C. Ospelkaus, S. Stahl, and D. Rodríguez, An optimized geometry for a micro Penning-trap mass spectrometer based on interconnected ions, Int. J. Mass Spectrom. **410**, 22 (2016).

[32] D. J. Wineland and W. M. Itano, Laser cooling of atoms, Phys. Rev. A **20**, 1521 (1979).

[33] J. M. Cornejo, R. Lehnert, M. Niemann, J. Mielke, T. Meiners, A. Bautista-Salvador, M. Schulte, D. Nitzschke, M. J. Borchert, K. Hammerer, S. Ulmer, and C. Ospelkaus, Quantum logic inspired techniques for spacetime-symmetry tests with (anti-)protons, New J. Phys. **23**, 073045 (2021).

[34] S. Jain, T. Sägesser, P. Hrmo, C. Torkzaban, M. Stadler, R. Oswald, C. Axline, A. Bautista-Salvador, C. Ospelkaus, D. Kienzler, and J. Home, Penning micro-trap for quantum computing, Nature (London) **627**, 510 (2024).

[35] M. Niemann, T. Meiners, J. Mielke, M. J. Borchert, J. M. Cornejo, S. Ulmer, and C. Ospelkaus, Cryogenic ^{9}Be$^+$ Penning trap for precision measurements with (anti-)protons, Meas. Sci. Technol. **31**, 035003 (2020).

[36] J. Mielke, J. Pick, J. A. Coenders, T. Meiners, M. Niemann, J. M. Cornejo, S. Ulmer, and C. Ospelkaus, 139 GHz UV phase-locked Raman laser system for thermometry and sideband cooling of ^{9}Be$^+$ ions in a Penning trap, J. Phys. B: At., Mol. Opt. Phys. **54**, 195402 (2021).

[37] D. Nitzschke, M. Schulte, M. Niemann, J. M. Cornejo, S. Ulmer, R. Lehnert, C. Ospelkaus, and K. Hammerer, Elementary laser-less quantum logic operations with (anti-)protons in Penning traps, Adv. Quantum Technol. **3**, 1900133 (2020).

[38] J. M. Cornejo, J. Brombacher, J. A. Coenders, M. Von Boehn, T. Meiners, M. Niemann, S. Ulmer, and C. Ospelkaus, Optical stimulated-Raman sideband spectroscopy of a single ^{9}Be$^+$ ion in a Penning trap, Phys. Rev. Res. **5**, 033226 (2023).

[39] T. Meiners, J. A. Coenders, J. Brombacher, M. Niemann, J. M. Cornejo, S. Ulmer, and C. Ospelkaus, Fast adiabatic transport of single laser-cooled ^{9}Be$^+$ ions in a cryogenic Penning trap stack, Eur. Phys. J. Plus **139**, 262 (2024).

[40] L. S. Brown and G. Gabrielse, Precision spectroscopy of a charged particle in an imperfect Penning trap, Phys. Rev. A **25**, 2423 (1982).

[41] T. Meiners, J.-A. Coenders, J. Mielke, M. Niemann, J. M. Cornejo, S. Ulmer, and C. Ospelkaus, Fast adiabatic transport of single laser-cooled ^{9}Be$^+$ ions in a cryogenic Penning trap stack, arxiv:2309.06776.

[42] S. Mavadia, G. Stutter, J. F. Goodwin, D. R. Crick, R. C. Thompson, and D. M. Segal, Optical sideband spectroscopy of a single ion in a Penning trap, Phys. Rev. A **89**, 032502 (2014).

[43] J. M. Cornejo, J.-A. Coenders, M. Niemann, T. Meiners, J. Mielke, A. Bautista-Salvador, R. Lehnert, S. Ulmer, and C. Ospelkaus, Towards resolved sideband laser cooling of single ^{9}Be$^+$ ions in a Penning trap for precision experiments with (anti-)protons, in *CPT and Lorentz Symmetry*, edited by R. Lehnert (World Scientific, Singapore, 2023), pp. 124–127.

[44] R. Bluhm, V. A. Kostelecký, and N. Russell, CPT and Lorentz tests in Penning traps, Phys. Rev. D **57**, 3932 (1998).

[45] V. A. Kostelecký and N. Russell, Data tables for Lorentz and *CPT* violation, Rev. Mod. Phys. **83**, 11 (2011).

[46] Y. Ding, Lorentz and *CPT* tests using Penning traps, Symmetry **11**, 1220 (2019).